Atmos. Chem. Phys. Discuss., 11, 8003–8025, 2011
www.atmos-chem-phys-discuss.net/11/8003/2011/
doi:10.5194/acpd-11-8003-2011

Atmospheric Chemistry and Physics Discussions

Evaluation of satellite-derived HCHO using statistical methods

J. H. Kim[1], S. M. Kim[1], K. H. Baek[1], L. Wang[2], T. Kurosu[3], I. De Smedt[4], K. Chance[3], and M. J. Newchurch[2]

[1]Department of Atmospheric Science, Pusan National University, Korea
[2]Department of Atmospheric Science, University of Alabama in Huntsville, USA
[3]Harvard-Smithsonian Center for Astrophysics, Harvard University, USA
[4]Belgian Institute for Space Aeronomy (BIRA-IASB), Brussels, Belgium

Received: 21 October 2010 – Accepted: 10 January 2011 – Published: 9 March 2011

Correspondence to: M. J. Newchurch (mike@nsstc.uah.edu)

Published by Copernicus Publications on behalf of the European Geosciences Union.

Abstract

Most previous evaluations of satellite performance relied on pair wise comparisons with limited spatial and temporal coverage of surface-based measurements such as soundings and in-situ measurements. Especially, validation of satellite HCHO measurements is very difficult because ground-based HCHO measurements are extremely sparse. We use a new scientific approach, statistical analyses with empirical orthogonal function (EOF) and singular value decomposition (SVD), to provide three-dimensional results of comparisons with a global picture over long measurement periods. The EOF and SVD analyses with GOME, SCIAMACHY and OMI HCHO, and MOPITT CO show dipole distributions oscillating between northern and southern equatorial Africa with an annual cycle. This feature is exactly coincident with the spatial and temporal pattern of biomass burning occurring over tropical Africa. The double-peaked maximum seen in OMI HCHO is only marginally observed in SCIAMACHY and GOME HCHO seasonality over the northern tropical region during northern biomass-burning season. Spatial and temporal difference between two datasets may cause this discrepancy, but the detailed analysis for the cause requires an examination with a chemical model. The statistical analyses of all data indicate that biomass-burning activity over South America is responsible for the HCHO seasonality over that continent. We have not observed any evidence to support the influence of biogenic activity on HCHO over these regions; however, we find robust evidence that biomass burning is the strongest source of HCHO over tropical Africa and South America. We also found that these statistical tools are a very efficient method for evaluating satellite data.

1 Introduction

Formaldehyde (HCHO) plays an important role in atmospheric chemistry as a tracer molecule in the production of the HO_x family, which is a major oxidizer throughout the entire atmosphere. HCHO is formed in the atmosphere as a result of atmospheric

ACPD
11, 8003–8025, 2011

oxidation of VOCs, including methane and isoprene, with loss from photolysis and reaction with OH. These processes result in HCHO having an extremely short lifetime (Palmer et al., 2006; Atkinson, 2000; Pfister et al., 2008; Stavrakou et al., 2009a, b; Dufour et al., 2009a). Atmospheric methane, which has a long lifespan, controls background levels of HCHO. In urban areas, anthropogenic VOCs are the most significant source in HCHO production, but biogenic VOCs are dominant elsewhere especially during the growing season, with the largest contribution coming from isoprene (Palmer et al., 2003; Millet et al., 2008; Dufour et al., 2009b). In addition, large sources of formaldehyde are directly emitted from biomass burning (Lee et al., 1997), incomplete combustion of fuels from mobile sources (de Serves, 1994), process emissions from oil refineries, and vegetation (Kesselmeier and Staudt, 1999; Lathière et al., 2006). As a result of various sources of VOCs, HCHO spatial and temporal distributions vary significantly across the globe.

The Global Ozone Monitoring Experiment (GOME) instrument, with a spatial resolution of $40 \times 320\,km^2$, provided global coverage of HCHO measurements from space for the first time in 1996 (Thomas et al., 1998). Due to improved spatial coverage from SCIAMACHY with 60×30 km and from OMI with 13×24 km, Chance (2000) and Kurosu (2008) have identified elevated HCHO concentrations associated with biogenic isoprene emissions, biomass burning, and urban pollution (Chance et al., 2000; Kurosu et al., 2008 De Smedt et al., 2008). These formaldehyde columns measured from space help to quantify the various VOC emissions used in chemical transport models (Palmer et al., 2006). In addition, these data reduce uncertainties in the budget of CO, which play a key role in controlling the abundance of tropospheric ozone and the hydroxyl radical (De Smedt et al., 2008).

Total-column HCHO, retrieved with the direct fitting of radiances, is based on non-linear least-squares fitting in the UV-A wavelength band. This algorithm was originally developed for GOME and adapted for the SCIAMACHY and OMI instruments. The results from the spectral fitting are HCHO slant columns, which are converted to vertical columns using a look-up table of air mass factors (AMFs) (Palmer et al., 2001; Kurosu

ACPD
11, 8003–8025, 2011

et al., 2008). Sources of error in the retrievals of vertical HCHO columns from GOME include: (1) the slant-column fitting, (2) the diffuser plate correction, and (3) the AMF calculation (Palmer et al., 2006). The retrieved HCHO measurement errors include influences from: (1) a latitudinal dependency of the background values that need to be corrected with a reference-sector method, (2) columns lower than the background level above desert regions, mainly Sahara and Australia and (3) features above oceans not predicted by chemical transport models (Wittrock et al., 2007; De Smedt et al., 2008; Stavrakou et al., 2009a).

Scientists have taken various approaches to validate retrieved data to quantify the errors and extract physically and chemically meaningful results. Validation techniques typically use a combination of satellite observations, in situ measurements, and chemistry and transport models, which represent the state of the atmosphere in different ways (Palmer et al., 2003, 2006; Abbot et al., 2003; Martin et al., 2004; Wittrock et al., 2007; Kurosu et al., 2008; Stavrakou et al., 2009a). However, validation of satellite HCHO measurements is very difficult because ground-based HCHO measurements are extremely sparse. This observation paucity hinders the construction of HCHO benchmarks over the globe for meaningful evaluation of the satellite measurements. Another difficulty in the evaluation derives from large uncertainties in the HCHO vertical columns, which typically range from 40–105% (Palmer et al., 2006; Kurosu et al., 2008). Therefore, without a detailed error map with respect to seasons and regions over the globe, the significant amount of uncertainty will prohibit our attempt to determine the top-down constraints on isoprene emission inventories, and thereby constrain our understanding of subsequent VOC-related atmospheric chemistry.

Inter-comparison between the satellite's HCHO measurements is challenging because HCHO retrievals from GOME are no longer reliable due to the advanced degradation of the GOME instrument. On the other hand, SCIAMACHY data is strongly influenced by instrument artifacts that render the retrieval of HCHO challenging. In evaluating consistency by comparing HCHO column measurements from the same season in different years, vertical columns retrieved from OMI over regions with enhanced

ACPD
11, 8003–8025, 2011

formaldehyde are in reasonable agreement with past observations from GOME and currently-retrieved SCIAMACHY observations (Kurosu et al., 2008). However, the comparisons have shown OMI columns over such hot-spots to be approximately 30% lower than GOME and SCIAMACHY (Kurosu et al., 2008). OMI HCHO columns over North America fall 2–14% below the curve defined by the ensemble of the GOME data (Millet et al., 2008). De Smedt et al. (2007) and Kurosu et al. (2008) indicated that only preliminary results from satellite HCHO inter-comparisons are available; so, a new method of satellite HCHO evaluation is required.

In this paper, we use a new scientific approach to provide three-dimensional results of comparisons with a global picture over long measurement periods. The tools used to evaluate satellite HCHO products are (1) the empirical orthogonal function (EOF) and (2) singular value decomposition (SVD). The EOF and SVD analysis approaches differ from the conventional ways of comparing patterns. Instead of using the typical pair wise station-to-station intercomparison, we perform the evaluation at the global scale using temporal and spatial patterns derived from the statistical analyses, which can provide three dimensional results. An additional advantage of these statistical approaches is that they enable us to evaluate the satellite HCHO measurements based on morphology and seasonality of HCHO emission sources and chemical process from various tropospheric constituents. This task can be achieved with these statistical tools by assessing the homogeneity of the satellite HCHO products derived from different platforms. In this approach, other satellite measurements linked to the HCHO distribution, such as biomass-burning fire counts, MOPITT (Measurements Of Pollution In The Troposphere) CO, and others, can be used jointly with the HCHO measurements to examine the consistency of their spatial and temporal patterns.

2 Method and data

Satellite instruments detect radiances resulting from scattering, reflection, and absorption/emission by the earth-atmosphere system. The measured radiances contain both

ACPD
11, 8003–8025, 2011

the desired signal from geophysical variables in the system and some noise. The signal-to-noise ratio strongly depends on the instrument and geophysical variables. Sophisticated retrieval algorithms can be used to determine a broad range of geophysical variables with limited signal-to-noise ratio. However, most are ill-posed retrievals requiring assumptions that must be justified with data. Therefore, there is always a need to validate the algorithms. Previous evaluations of satellite performance have relied on comparisons with limited spatial and temporal coverage of surface-based measurements such as soundings and in-situ measurements. However, the levels of agreement from these comparisons vary according to location and season, so there has been no clear superior method among various satellite HCHO products. This ambiguity motivates the requirement for a better method of evaluating satellite products.

Our approach is to validate the satellite retrievals by analyzing individual satellite products as well as a combination of two kinds of satellite products linked in both spatial and temporal domains. EOF analysis is a promising statistical tool for identifying these coupled relationships with spatial and temporal patterns of individual parameters. SVD works well when combining the two parameters (Venegas et al., 1997; Yun and Kwon, 2002). The result of these techniques is the extraction of the dominant characteristics of a parameter's spatial and temporal patterns with discrimination between the signal of interest and unrelated processes or noise.

The EOF method analyzes the variability of a single field, finds the spatial patterns of variability (called the EOFs), its time variation (called the EOF time series or expansion coefficients), and gives a quantitative measure of the importance of each pattern. The SVD method examines the coupled variability of two fields. Each pair of singular vectors describes a fraction of the square covariance (SCF) between the two variables. The first mode describes the largest SCF, and each succeeding pair describes the maximum remaining SCF that is unexplained by the previous pairs (Venegas et al., 1997).

ACPD
11, 8003–8025, 2011

For these analyses, we use GOME, SCIAMACHY (http://www.temis.nl/airpollution/ch2o.html), and OMI HCHO (http://mirador.gsfc.nasa.gov) along with MOPITT CO (ftp://l4ftl01.larc.nasa.gov/MOPITT) measurements for SVD analyses that compare covariance with HCHO measurements.

OMI flies on NASA's Aura satellite platform in a sun-synchronous orbit with a 01:45 p.m. equator-crossing time (ascending node). HCHO total columns are retrieved from reflected sunlight observed in nadir. The retrieval algorithm is based on non-linear least squares fitting of radiances in the spectral region of 327.5–356.5 nm. The spectral fitting provides slant columns, which are converted to vertical columns using air mass factors computed with a multiple-scattering radiative transfer model (Spurr et al., 2001) and based on GEOS-Chem seasonal HCHO climatologies (Palmer et al., 2001). Typical column uncertainties of the operational OMI HCHO product range of 50% to 100%.

The OMI HCHO columns used in this study are taken from the operational (NASA HCHO), modified for an apparent increase of background values over the OMI lifetime that was discovered in the process of the current analysis. Figure 1 shows monthly averages of OMI HCHO over the remote Pacific from September 2004 to September 2009, which clearly exhibit visible positive trend in the data. The reason for this trend is currently under investigation, but it is very likely connected to a similar increase in detector dark current observed over the OMI lifetime (Jaross, 2009) HCHO is the weakest absorber operationally retrieved from OMI and hence the first to show effects related to instrument degradation. Figure 1 also shows a background parameterization derived from a 4th order polynomial fit to the time series of monthly average HCHO data. This parameterization corrected the OMI HCHO data that went into the analysis presented here. Numerical results quoted in tables and the main texts are based on the corrected data. Cloud screening was applied to OMI HCHO data, and all ground pixels with cloud cover greater than 40% were rejected in the averaging.

The data periods range from April 1996 to June 2003 for GOME HCHO; from January 2003 to December 2008 for SCIAMACHY; from October 2004 to December 2008 for

ACPD
11, 8003–8025, 2011

OMI HCHO; and from March 2000 to December 2008 for MOPITT. All HCHO data were rejected for cloud cover greater than 40%.

3 Results

Figure 2 shows the EOF analyses of OMI, GOME, and SCIAMACHY HCHO along with MOPITT CO data over Africa. The left and right columns in the figure show the maps of spatial patterns and the coupled time series of the expansion coefficients with squared covariance fractions in mode one, respectively. The time expansion coefficient (red dashed line) is the monthly average over the entire period, which repeats every year for comparison.

The spatial and temporal patterns of MOPITT CO from EOF mode 1 in Fig. 2a show a well-defined north-south dipole oscillation, with a distinctive annual cycle of the northern maximum between December and April and the southern maximum between August and October. These patterns are well-correlated with those from total fire counts between 2000 and 2009, which were measured by the Along-Track Scanning Radiometer (ATSR) (http://www.atsr.rl.ac.uk/). The dipole distribution of fire is evident between northern and southern tropical Africa with about the same intensity as MOPITT CO. The peaks of fire counts and CO occur in January and March–April over the northern tropics, and in the July and September-October period over southern tropics. The time lag between the two is likely due to the longer lifetime of CO in the atmosphere. The location of maximum CO shifts slightly westward from the location of the maximum fire counts. This shift could originate from the transport of CO with the prevailing easterly in the tropical region. Therefore, biomass burning is the main driving mechanism for CO over this region.

The spatial patterns and time series of corrected OMI HCHO data in Fig. 2b have much in common with MOPITT CO. The background parameterization removed the unrealistic trend and cloud screening improved the spatial coherence between OMI HCHO and MOPITT CO. The EOF mode 1 of both datasets explains about 58% and 48% of the total variance, respectively. We observe the same north-south dipole

ACPD
11, 8003–8025, 2011

oscillation with a distinct annual cycle from both datasets. The locations of maximum HCHO and CO agree well with the fire counts over south central Africa for the southern burning season. Maximum burning was observed in July followed by maximum HCHO in August and maximum CO during the September–October period over southern Africa. This time sequence agrees with the lifetime between HCHO and CO. However, some discrepancies between the two species are found in the spatial and temporal patterns during the northern biomass-burning season. It is expected that maximum HCHO rather than CO should be observed closer to north central equatorial Africa, where more intensive burning takes place, because of a shorter lifetime of HCHO relative to CO. Conversely, the observations revealed that the maximum HCHO was found further downwind from where maximum CO was observed. In addition, the fire counts show that burning is the highest in January during the northern burning season (http://www.atsr.rl.ac.uk/); whereas, HCHO shows a temporary minimum in January between two peaks in December and March. These spatial and temporal patterns are different from those seen over southern tropical Africa during the southern burning season.

The EOF mode 1 of SCIAMACHY and GOME HCHO explains only little more than 20% of the total variance shown in Fig. 2c and 2d. The HCHO signals are the strongest in the west where maximum fire counts occur downwind. However, maximum OMI HCHO is observed further downwind where maximum SCIA and GOME HCHO are found during the northern biomass-burning season.

A significant difference between SCIAMACHY, GOME and OMI HCHO comes from the seasonality observed in the northern tropical region during the northern biomass-burning season. The double-peak feature seen in OMI HCHO seasonality is marginally observed in SCIAMACHY and GOME HCHO seasonality. The difference in HCHO seasonality between datasets could be caused by the difference in spatial and temporal resolution between the instruments. However, this explanation does not seem to be the likely cause because the difference in seasonality is observed over a large area and for many years. Analyzing climatological wind and precipitation over this region reveals

ACPD
11, 8003–8025, 2011

that the wind is northeasterly and the ITCZ is located in south of the equator during the boreal winter. No special weather pattern was observed over northern tropical Africa in January (http://iridl.ldeo.columbia.edu/maproom/.Regional/.Africa). Another possibility for the cause could be the difference in equator crossing time between OMI (01:45 p.m.), and SCIAMACHY (10:00 a.m.). (http://www.knmi.nl; http://envisat.esa.int). The diurnal cycle of biomass-burning activity and HCHO-related chemistry may be the cause of the difference (Benning and Wahner, 1998; Palmer et al., 2007; Stavrakou et al., 2009a), but a detailed chemical analysis is beyond the scope of this study.

Because sufficient amounts of isoprene, which will eventually turn to HCHO through the photochemical oxidation process, are released from biogenic activity in the African rainforest, it would be interesting to analyze how biogenic activity influences HCHO seasonality over Africa. The African rainforest is located over the west equatorial region 7° N–7° S and 10°–30° E, and shows a clear semi-annual cycle with peaks during the rainy seasons (October–December and March–May) and minima during the dry seasons (June–September, January–February), although rainfall is clearly substantial in all seasons (Todd et al., 2003; Sultan and Janicot, 2000). This shift of the rainy season over the rainforest is basically associated with the north/south movement of the ITCZ across equatorial tropical Africa. If biogenic activity is comparable with biomass burning, we should be able to observe a noticeable signal over the rainforest region in west equatorial Africa from the spatial distribution of EOF mode 1 in Fig. 2. However, a meaningful signal was not detected over the rainforest region. Rather, the spatial and temporal patterns are consistent with those of biomass burning deduced from CO.

For further evaluation, we performed SVD analysis to examine the detailed relationship of coupled variables between HCHO and CO. For this analysis, SCIMACHY HCHO was selected because it has a similar measurement period to OMI HCHO. Figure 3a shows the first mode of the SVD between OMI HCHO and MOPITT CO. The spatial correlation map shows remarkable agreement between the two gases. This mode explains 63% of the total square covariance with a correlation coefficient of 0.82. Even

ACPD
11, 8003–8025, 2011

though a slight local minimum is observed in January from OMI HCHO, overall, the time series shows a well-defined annual cycle that is consistent with the biomass-burning cycle shown in the EOF analysis. These good spatial and temporal correlations along with EOF and SVD analyses suggest that biomass burning is the major driving source of HCHO and CO over Africa as of analyses of EOF and SVD.

Figure 3b shows the first mode of the SVD between SCIAMACHY HCHO and MOPITT CO. This mode explains 47% of the total square covariance with correlation coefficient of 0.86. The spatial and temporal coherence between two gases are very similar with those results shown in Fig. 3a. These analyses suggest that the source of HCHO is strongly linked to biomass burning.

Figure 4 shows the EOF mode 1 of the satellite measurements over South America. The spatial pattern shows a unique maximum over southern equatorial South America with a peak in September. The first mode of CO and OMI HCHO explains most of the total variance, but GOME and SCIAMACHY HCHO explain less than 20% due to spatial and temporal resolution lower than OMI. Even though fire activity is observed over northern equatorial South America, the strength and coverage is far less than those from the southern equatorial South American fire counts. The spatial and temporal patterns of all measurements are very consistent with the fire counts shown in (http://www.atsr.rl.ac.uk/).

As for chemical source evaluation in Africa, we examined the role of biogenic activity over the Amazon rainforest. If CO and HCHO from biogenic activity played a comparable role relative to biomass-burning activity, we should be able to observe the signal over the Amazon rainforest in the area of 5° N–5° S from the EOF spatial pattern in Fig. 4. However, we have not observed any noticeable signal from the Amazon rainforest region that could cause any impact on EOF of CO and HCHO. This result is consistent with Williams et al. (2001) who showed that CO production from oxidation of isoprene from the rainforest is much less than the observed CO. They concluded that observed CO over the Amazon rainforest was transported primarily with the prevailing easterly from savanna fires in South America.

ACPD
11, 8003–8025, 2011

The first mode of the CO and HCHO from the SVD analyses explains most of the total square variance shown in Fig. 5. The spatial and temporal coherences between CO and HCHO show the robust evidence that biomass burning is the main driving mechanism for HCHO over South America as we have seen over Africa.

4 Conclusions

Most previous evaluations of satellite performance relied on pair wise comparisons with limited spatial and temporal coverage of surface-based measurements such as soundings and in-situ measurements. When individual satellite HCHO measurements contain significant amounts of error, it poses additional challenges during evaluation due to the intrinsic errors already associated with differences in location and season. In order to overcome this problem, we suggest a new way of satellite data evaluation with statistical tools such as empirical orthogonal functions and singular value decomposition analysis.

The EOF and SVD analyses with GOME, SCIAMACHY and OMI HCHO, and MOPITT CO show dipole distributions oscillating between northern and southern equatorial Africa with an annual cycle. This feature is exactly coincident with the spatial and temporal pattern of biomass burning occurring over tropical Africa. The double-peaked maximum seen in OMI HCHO is only marginally observed in SCIA and GOME HCHO seasonality over the northern tropical region during northern biomass-burning season. Spatial and temporal difference between two datasets may cause this discrepancy, but the detailed analysis for the cause requires an examination with a chemical model. The statistical analyses of all data indicate that biomass-burning activity over South America is responsible for the HCHO seasonality over that continent.

We have not observed any evidence to support the influence of biogenic activity on HCHO over these regions; however, we find robust evidence that biomass burning is the strongest source of HCHO over tropical Africa and South America. We also found that these statistical tools are a very efficient method for evaluating satellite data.

ACPD
11, 8003–8025, 2011

Acknowledgements. This work was supported by NASA and the Korea Meteorological Admistration (RACS 2010-1011).

References

Abbot, D. S., Palmer, P. I., Martin, R. V., Chance, K. V., Jacob, D. J., and Guenther, A.: Seasonal and interannual variability of North American isoprene emissions as determined by formaldehyde column measurements from space, Geophys. Res. Lett., 30, 1886, doi:10.1029/2003GL017336, 2003.

Atkinson, R.: Atmospheric chemistry of VOCs and NO_x, Atmos. Environ., 34, 2063–2101, 1352-2310/00, 2000.

Benning, L. and Wahner, A.: Measurements of atmospheric formaldehyde (HCHO) and acetaldehyde (CH3CHO) during POPCORN 1994 using 2.4-DNPH coated silica cartridges, J. Atmos. Chem., 31, 105–117, 1998.

Chance, K., Palmer, P., Spurr, R. J. D., Martin, R. V., Kurosu, T., and Jacob, D. J.: Satellite observations of formaldehyde over North America from GOME, Geophys. Res. Lett., 27, 3461–3464, 2000.

de Serves, C.: Gas phase formaldehyde and peroxide measurements in the Arctic atmosphere, J. Geophys. Res., 99, 25391–25398, doi:10.1029/94JD00547, 1994.

De Smedt, I., Roozendael, M. V., Stavrakou, T., Müller, J.-F., Van der A, R., and Eskes, H.: Global observations of formaldehyde in the troposphere by satellites: GOME and SCIAMACHY Results, Proc. Envisat Symposium, Montreux, Switzerland, 2007,

De Smedt, I., Müller, J.-F., Stavrakou, T., van der A, R., Eskes, H., and Van Roozendael, M.: Twelve years of global observations of formaldehyde in the troposphere using GOME and SCIAMACHY sensors, Atmos. Chem. Phys., 8, 4947–4963, doi:10.5194/acp-8-4947-2008, 2008.

Dufour, G., Wittrock, F., Camredon, M., Beekmann, M., Richter, A., Aumont, B., and Burrows, J. P.: SCIAMACHY formaldehyde observations: constraint for isoprene emission estimates over Europe?, Atmos. Chem. Phys., 9, 1647–1664, doi:10.5194/acp-9-1647-2009, 2009a.

Dufour, G., Szopa, S., Barkley, M. P., Boone, C. D., Perrin, A., Palmer, P. I., and Bernath, P. F.: Global upper-tropospheric formaldehyde: seasonal cycles observed by the ACE-FTS

ACPD

11, 8003–8025, 2011

satellite instrument, Atmos. Chem. Phys. Discuss., 9, 1051–1095, doi:10.5194/acpd-9-1051-2009, 2009b.
Kesselmeier, J. and Staudt, M.: Biogenic volatile organic compounds (VOC): An overview on emission, physiology, and ecology, J. Atmos. Chem., 33, 23–88, 1999.
Kurosu, T. P., Liu, X., Celarier, E. A., and Chance, K.: Air Quality Observations from the Ozone Monitoring Instrument on EOS/Aura - HCHO and CHO-CHO, Proceedings of the American Geophysical Union Joint Assembly, 2008.
Lathière, J., Hauglustaine, D. A., Friend, A. D., De Noblet-Ducoudré, N., Viovy, N., and Folberth, G. A.: Impact of climate variability and land use changes on global biogenic volatile organic compound emissions, Atmos. Chem. Phys., 6, 2129–2146, doi:10.5194/acp-6-2129-2006, 2006.
Lee, M., Heikes, B. G., Jacob, D. J., Sachse, G., and Anderson, B.: Hydrogen peroxide, organic hydroperoxide, and formaldehyde as primary pollutants from biomass burning, J. Geophys. Res., 102, 1301–1309, doi:10.1029/96JD01709, 1997.
Martin, R. V., Parrish, D. D., Ryerson, T. B., Jr., D. K. N., Chance, K., Kurosu, T. P., Jacob, D. J., Sturges, E. D., Fried, A., and Wert, B. P.: Evaluation of GOME satellite measurements of tropospheric NO_2 and HCHO using regional data from aircraft campaigns in the southeastern United States, J. Geophys. Res., 109, D24307, doi:10.1029/2004JD004869, 2004.
Millet, D. B., Jacob, D. J., Boersma, K. F., Fu, T.-M., Kurosu, T. P., Chance, K., Heald, C. L., and Guenther, A.: Spatial distribution of isoprene emissions from North America derived from formaldehyde column measurements by the OMI satellite sensor, J. Geophys. Res., 113, D02307, doi:10.1029/2007JD008950, 2008.
NASA HCHO, Operational OMI HCHO data product: http://disc.sci.gsfc.nasa.gov/Aura/data-holdings/OMI/omhcho_v003.shtml, 2010.
Palmer, P. I., Jacob, D. J., Chance, K., Martin, R. V., Spurr, R. J. D., Kurosu, T. P., Bey, I., Yantosca, R., Fiore, A., and Li, Q.: Air mass factor formulation for spectroscopic measurements from satellites: Application to formaldehyde retrievals from the Global Ozone Monitoring Experiment, J. Geophys. Res., 106, 14539–14550, doi:10.1029/2000JD900772, 2001.
Palmer, P. I., Jacob, D. J., Fiore, A. M., Martin, R. V., Chance, K., and Kurosu, T. P.: Mapping isoprene emissions over North America using formaldehyde column observations from space, J. Geophys. Res., 108, 4180, doi:10.1029/2002JD002153, 2003.
Palmer, P. I., Abbot, D. S., Fu, T.-M., Jacob, D. J., Chance, K., Kurosu, T. P., Guenther, A., Wiedinmyer, C., Stanton, J. C., Pilling, M. J., Pressley, S. N., Lamb, B., and Sumner, A. L.:

ACPD
11, 8003–8025, 2011

Quantifying the seasonal and interannual variability of North American isoprene emissions using satellite observations of the formaldehyde column, J. Geophys. Res., 111, D12315, doi:10.1029/2005JD006689, 2006.

Palmer, P. I., Barkley, M. P., Kurosu, T. P., Lewis, A. C., Saxton, J. E., Chance, K., and Gatti, L. V.: Interpreting satellite column observations of formaldehyde over tropical South America, Phil. Trans. R. Soc., 365, 1741–1751, doi:10.1098/rsta.2007.2042, 2007.

Pfister, G. G., Emmons, L. K., Hess, P. G., Lamarque, J.-F., Orlando, J. J., Walters, S., Guenther, A., Palmer, P. I., and Lawrence, P. J.: Contribution of isoprene to chemical budgets: A model tracer study with the NCAR CTM MOZART-4, J. Geophys. Res., 113, D05308, doi:10.1029/2007JD008948, 2008.

Spurr, R. J. D., Kurosu, T. P., and Chance, K. V.: A linearized discrete ordinate radiative transfer model for atmospheric remote-sensing retrieval, J. Quant. Specrosc. Ra., 68, 689–735, 2001.

Stavrakou, T., Müller, J.-F., De Smedt, I., Van Roozendael, M., van der Werf, G. R., Giglio, L., and Guenther, A.: Evaluating the performance of pyrogenic and biogenic emission inventories against one decade of space-based formaldehyde columns, Atmos. Chem. Phys., 9, 1037–1060, doi:10.5194/acp-9-1037-2009, 2009.

Stavrakou, T., Müller, J.-F., De Smedt, I., Van Roozendael, M., van der Werf, G. R., Giglio, L., and Guenther, A.: Global emissions of non-methane hydrocarbons deduced from SCIAMACHY formaldehyde columns through 20032006, Atmos. Chem. Phys., 9, 3663-3679, doi:10.5194/acp-9-3663-2009, 2009b.

Strik, H. and Boves, L.: Fundamental frequency and intensity control in speech, J. Acous. Soc. Am., 82, S17(A), 1987.

Sultan, B. and Janicot, S.: Abrupt shift of the ITCZ over West Africa and intra-seasonal variability, Geophys. Res. Lett., 27, 3353–3356, 2000.

Thomas, W., Hegels, E., Slijkhuis, S., Spurr, R., and Chance, K.: Detection of biomass burning combustion products in Southeast Asia from backscatter data taken by the GOME spectrometer, Geophys. Res. Lett., 25, 1317–1320, 1998.

Todd, M. C., Washington, R., and James, T.: Characteristics of summertime daily rainfall variability over South America and the South Atlantic Convergence Zone, Meteor. Atmos. Phys., 83, 89–108, doi:10.1007/s00703-002-0563-9, 2003.

Venegas, S. A., Mysak, L. A., and Straub, D. N.: Atmosphere-ocean coupled variability in the South Atlantic, J. Climate, 10, 2904–2920, 1997.

ACPD

11, 8003–8025, 2011

Williams, J., Fischer, H., Hoor, P., Pöschl, U., Crutzen, P. J., Andreae, M. O., and Lelieveld, J.: The influence of the tropical rainforest on atmospheric CO and CO_2 as measured by aircraft over Surinam, South America, Chemosphere-Global Change Science, 3, 157–170, doi:10.1016/S1465-9972(00)00047-7, 2001.

Wittrock, F., Richter, A., Vrekoussis, M., and Burrows, J. P.: Global Observations of Formaldehyde and Glyoxal from Space, Contribution to the ACCENT Workshop on Volatile Organic Compounds: Group 2, ACCENT Secretariat, 2007.

Yun, W. T. and Kwon, W. T.: SVP multi-model super ensemble technique for long-term prediction, Korean J. Atmos. Sci., 5, 217–228, 2002.

ACPD

11, 8003–8025, 2011

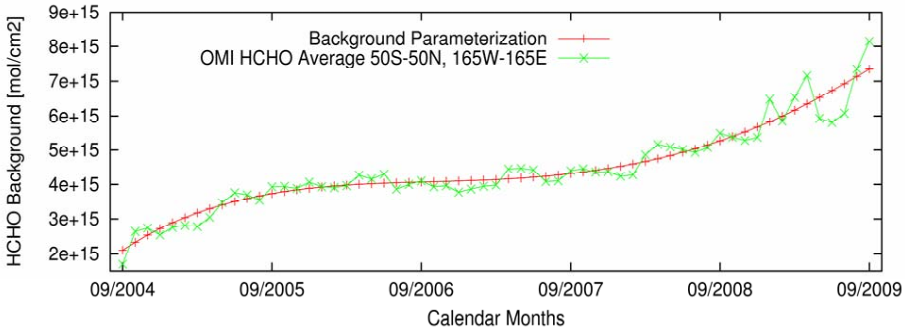

Fig. 1. Monthly averages of OMI HCHO background values (green line) from September 2004 through September 2009 over the remote Pacific (50° N–50° S, 165° W–165° E), and a parameterization (red line) using a 4th order polynomial fit to the monthly averages.

ACPD
11, 8003–8025, 2011

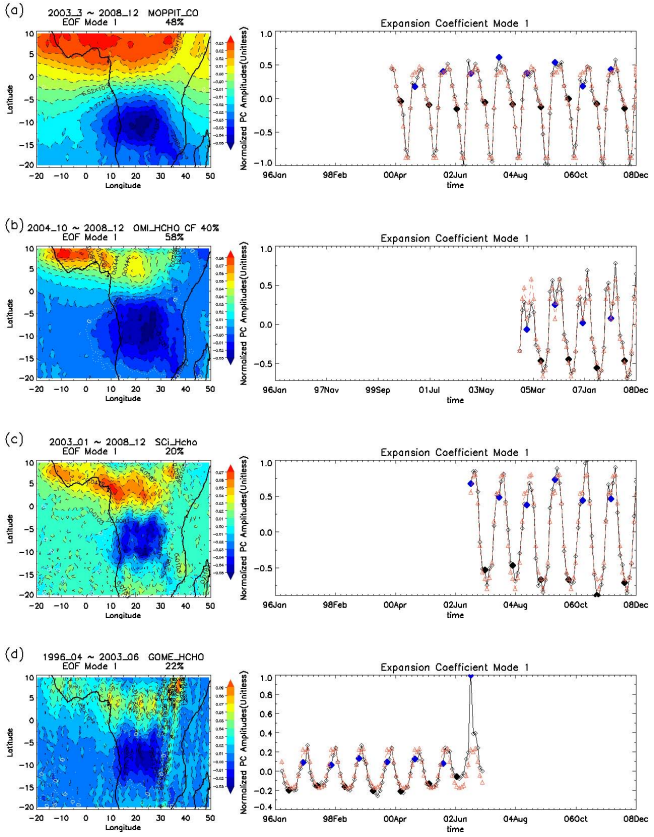

Fig. 2. EOF analyses of MOPITT CO, OMI HCHO, GOME, HCHO and SCIAMACHY HCHO over Africa. The red line represents the monthly average over entire measurement period. The blue and black dots correspond to the month of January and July, respectively.

ACPD
11, 8003–8025, 2011

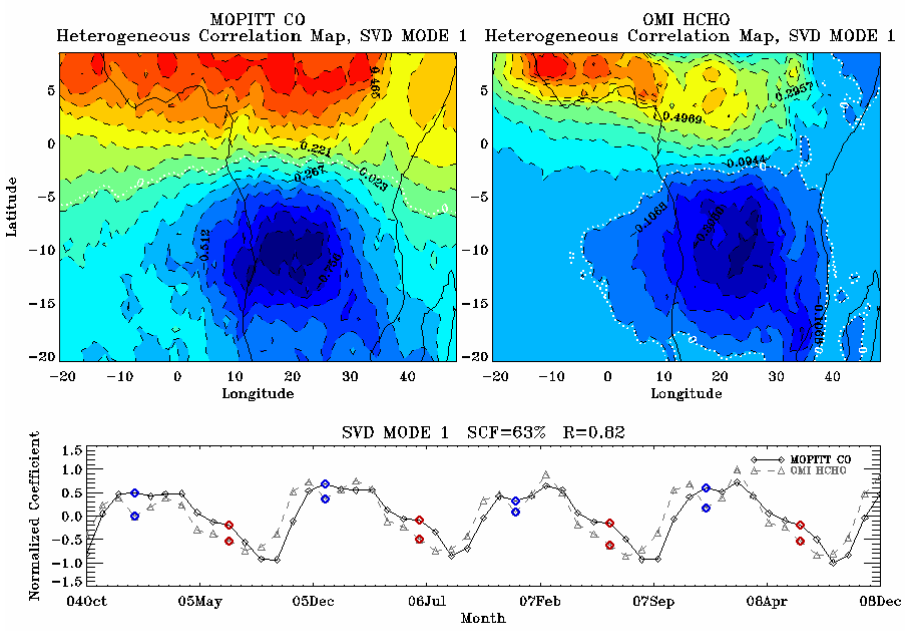

Fig. 3a. The first mode of the SVD between OMI HCHO and MOPITT CO. The dark color represents MOPITT CO and light color represents OMI HCHO. The blue and black dots correspond to the month of January and July, respectively.

ACPD
11, 8003–8025, 2011

Evaluation of satellite-derived HCHO using statistical methods

J. H. Kim et al.

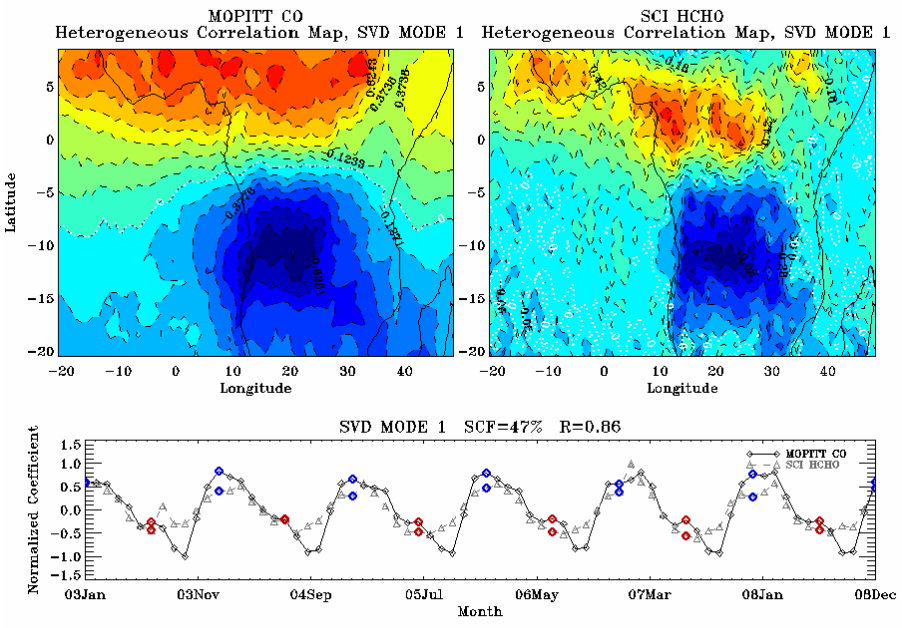

Fig. 3b. The first mode of the SVD between SCIAMACHY HCHO and MOPITT CO. The dark color represents MOPITT CO and light color represents SCIAMACHY HCHO. The blue and black dots correspond to the month of January and July, respectively.

ACPD
11, 8003–8025, 2011

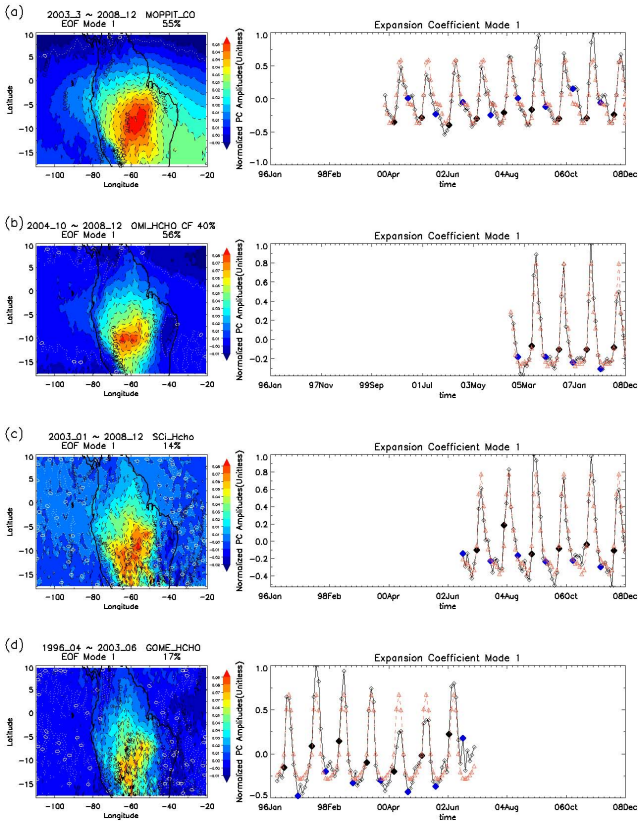

Fig. 4. EOF analyses of MOPITT CO, OMI, GOME, and SCIAMACHY HCHO over South America. The red line represents monthly average over the entire measurement period. The blue and black dots correspond to the month of January and July, respectively.

ACPD
11, 8003–8025, 2011

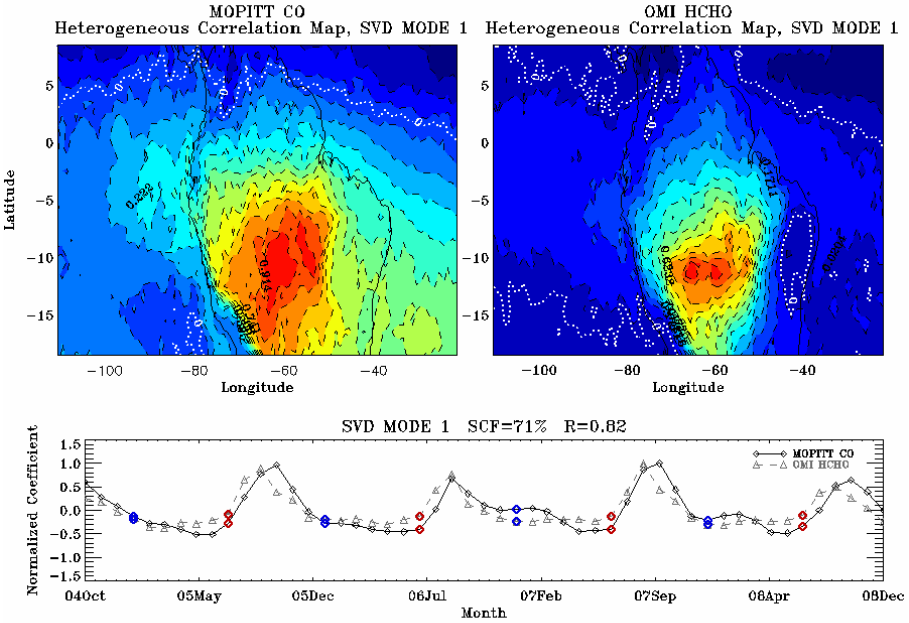

Fig. 5a. The first mode of the SVD between OMI HCHO and MOPITT CO over South America. The dark color represents MOPITT CO and light color represents OMI HCHO. The blue and black dots correspond to the month of January and July, respectively.

ACPD
11, 8003–8025, 2011

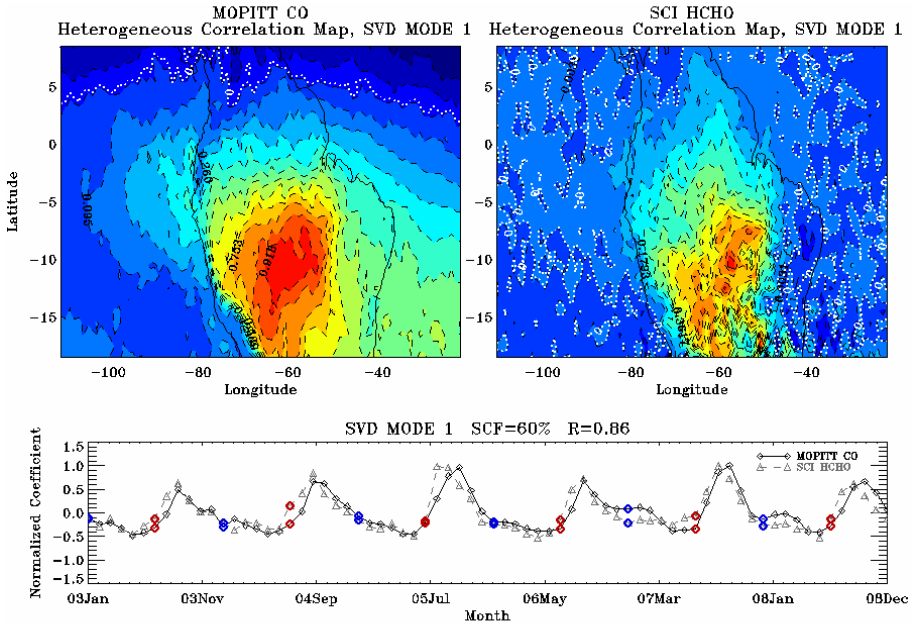

Fig. 5b. The first mode of the SVD between SCHIAMACHY HCHO and MOPITT CO over South America. The dark color represents MOPITT CO and light color represents SCIAMACHY HCHO. The blue and black dots correspond to the month of January and July, respectively.

ACPD
11, 8003–8025, 2011